IOP Conf. Series: Materials Science and Engineering **418** (2018) 012037 doi:10.1088/1757-899X/418/1/012037

A simplified stress-based forming limit criterion for advanced high strength steel (AHSS)

B M Hance and L Huang

United States Steel Corporation, 5850 New King Court, Troy, MI 48098, USA

bhance@uss.com

Abstract. A methodology for stress-based forming limit analysis has been developed for advanced high strength steel (AHSS). It was proposed that localized necking occurs when a critical normal stress condition is met. Using a basic, isotropic material model (von Mises, power law hardening), the criterion was applied to various 980 Class AHSS. In most cases the simplified criterion adequately described the experimental strain-based forming limit curve (FLC). For AHSS with substantial volume fractions of metastable austenite, a more sophisticated material model and/or an adapted failure criterion will be required. A strong linear relationship was found between the critical normal stress and the measured true stress at maximum load in tension. This empirical functionality applies over a large range of strength levels and may form the basis for a methodology by which FLCs may be estimated from standard tension tests. Finally, in the context of the proposed failure criterion, the effects of work hardening behavior on the "shape" of the strain-based FLC are explored.

1. Introduction

1.1. Stress-based forming limits

While an exhaustive review of sheet metal forming limit criteria is beyond the scope of this paper, the authors refer the reader to the compendium of Stoughton and Yoon [1] for more information. A brief timeline of strain-based and stress-based forming limit concept development follows.

In 1964 Keeler and Backhofen [2] introduced the strain-based forming limit curve (FLC), and in the late 1960s, Nakazima *et al*. [3] first indicated the *dynamic* nature of strain-based FLCs. That is, strain-based FLCs generated under rectilinear strain path conditions generally do not apply to more complex, non-linear strain paths. In 1977 Kleemola and Pelkkikangas [4] first suggested that an intrinsic *stress*-based forming limit criterion exists—*i.e.* independent of strain path. Arrieux *et al*. [5] revealed the first compelling experimental evidence of a stress-based forming limit in 1982 and continued to develop this concept into the mid-1990s [6].

In the early 2000s, Stoughton revived stress-based formability assessment [7], where various researchers followed, *e.g.* [8]-[15]. A common approach is to transform an experimental strain-based FLC from strain space to stress space with known plane-stress plasticity relationships to achieve a stress-based forming limit curve (hereafter FLC_σ). Panich *et al.* [16] used a similar approach to transform a strain-based *fracture* forming limit curve (FFLC) to a stress-based FFLC.

Stoughton [16] explained that "the shape and location of the FLC in stress space" depends on the material model used for the strain-stress transformation. However, it was also explained that "the

degeneracy of the path-dependent strain-based curves to a single curve in stress space is such a strong physical phenomenon that it manifests itself in all material models tested." Building upon work of Sing and Rao [18] , Matin *et al.* [8] recognized that FLC_σ may be approximated by a "straight horizontal forming limit curve in two-dimensional principal stress space." In other words the forming limit is reached when σ_1 (or σ_2) reaches a critical value, regardless of deformation history.

1.2. Scope

In this analysis a simplified, stress-based forming limit criterion is proposed for advanced high strength steel (AHSS). After the suggestion of Matin *et al.* [8], it is assumed that localized necking occurs when a critical normal stress criterion is met. For added simplicity the von Mises yield function and power law work hardening are assumed. The applicability of the proposed criterion is assessed by fitting the forming limit model to experimental strain-based FLCs of 980 class AHSS materials.

2. Background

2.1. Material model

For plane stress ($\sigma_3 = 0$), the von Mises expression for effective stress ($\bar{\sigma}$) is often expressed as [10]:

$$\bar{\sigma} = \sigma_1(1 - \alpha + \alpha^2)^{0.5} = \sigma_1 A, \tag{1}$$

where α is the principal stress ratio σ_2/σ_1. In terms of total plastic strains, the effective strain ($\bar{\varepsilon}$) is:

$$\bar{\varepsilon} = \varepsilon_1 \left[\frac{4}{3}(1 + \beta + \beta^2)\right]^{0.5} = \varepsilon_1 B, \tag{2}$$

where β is the principal strain ratio $\varepsilon_2/\varepsilon_1$. The major strain ($\varepsilon_1$) and minor strain ($\varepsilon_2$) are aligned with σ_1 and σ_2, respectively, and ε_3 is the thickness strain. For von Mises, the plane-stress flow rule gives:

$$\beta = \frac{2\alpha - 1}{2 - \alpha}. \tag{3}$$

Furthermore, for "power law" work hardening, effective stress and effective strain are related by:

$$\bar{\sigma} = K\bar{\varepsilon}^n \;\rightarrow\; \sigma_1 A = K(\varepsilon_1 B)^n, \tag{4}$$

where *K* is the strength coefficient, and *n* is the work hardening exponent.

2.2. Stress-based forming limit criterion

It is now assumed that localized necking occurs when σ_1 reaches a critical value ($\sigma_1 = \sigma^*$). By rearranging Equation (4), an expression for major strain at the forming limit is obtained:

$$\varepsilon_1 = \frac{1}{B}\exp\left[\frac{\ln(\sigma^* A K^{-1})}{n}\right]. \tag{5}$$

Thus, the entire FLC may now be mapped into strain space with knowledge of the power law coefficients (n, K) and the critical normal stress (σ^*). For principal stress ratios ranging from $\alpha = 0$ (uniaxial tension) to $\alpha = 1$ (balanced biaxial tension), the effect of n on the predicted strain-based FLC is shown in Figure 1, where σ^* (unknown) is assumed equal to K. As n decreases, the FLC assumes a sharper V shape. A similar shape-dependence on n is captured in the classical deformation theory of Stören and Rice [19]-[21] and is often reflected in experimental data [22]-[24]. Furthermore, prior deformation (pre-strain) invariably results in a sharper V shape for the resultant FLC when

compared to non-pre-strained material—presumably accompanied by lower n values in the pre-strained condition [6], [9], [13]-[14], [16]. In Figure 1, n = 0.1 and n = 0.25 are realistic work hardening exponents for advanced high strength steels and mild steels, respectively. The absurd values n = 1 and n = 100 are included simply as further exploration of the relationship between n and the shape of the strain-based FLC with respect to the proposed failure criterion and the assumed material model. For n = 1, the FLC becomes linear. For n > 1 the FLC exhibits *downward* curvature, and for n >> 1 the FLC assumes asymptotically the form shown in Figure 1 for n = 100. As n approaches zero (not shown), the plane-strain forming limit (ε_1 at ε_2 = 0) approaches zero accordingly.

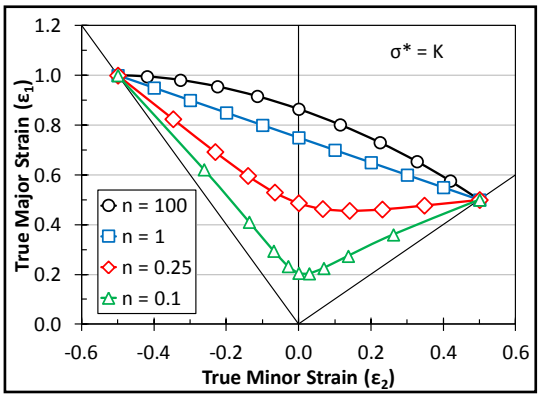

Figure 1. Theoretical effect of the work hardening exponent (n) on the strain-based forming limit curve. Here it is assumed that the critical normal stress (σ^*) is equal to the strength coefficient (K). See text for details.

Figure 2 shows the relationship between the expanded von Mises plane stress yield locus (isotropic hardening) and the proposed failure criterion in the tension-tension quadrant. Here the yield locus has intersected the failure "square" in plane strain, and it is assumed that σ^* is the same in the σ_1 and σ_2 direction. The yield locus is inside the square for other stress states at the same equivalent strain. In other words, failure occurs at the lowest effective strain in plane strain. This observation, in part, accounts for the V shape of the strain-based forming limit curve for realistic values of n (Figure 1). Table 1 shows stress-strain relationships for various plane-stress deformation modes at $\sigma_1 = \sigma^*$.

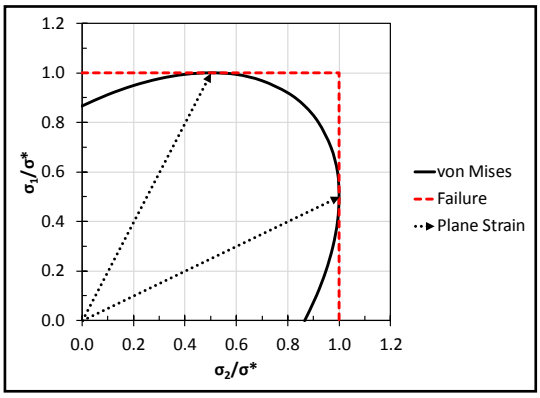

Figure 2. Tension-tension quadrant of the expanded von Mises plane stress yield locus (isotropic hardening), where σ_1 and σ_2 are normalized to the critical normal stress (σ^*). Here σ_1 and σ_2 have reached σ^* in plane strain for $\sigma_2/\sigma_1 = 0.5$ and 2.0, respectively (arrows).

Table 1. Stress-strain relationships for various plane-stress deformation modes ($\sigma_1 = \sigma^*$)

Mode[a]	α	β	$\bar{\sigma}$	$\bar{\varepsilon}$	ε_1
UT	0	-0.5	σ^*	$\exp\left[\frac{\ln(\sigma^*/\mathrm{K})}{n}\right] = \bar{\varepsilon}_{\mathrm{UT}}$	$\bar{\varepsilon}_{\mathrm{UT}}$
PS	0.5	0	$(\sqrt{3}/2)\sigma^*$	$\exp\left\{\frac{\ln\left[(\sqrt{3}/2)\sigma^*/K\right]}{n}\right\} = \bar{\varepsilon}_{\mathrm{PS}}$	$(\sqrt{3}/2)\bar{\varepsilon}_{\mathrm{PS}}$
BB	1	1	σ^*	$\bar{\varepsilon}_{\mathrm{UT}}$	$(1/2)\bar{\varepsilon}_{\mathrm{UT}}$

[a] UT = uniaxial tension, PS = plane strain, BB = balanced biaxial stretching

Figure 3 illustrates the sigmoidal relationship between the work hardening exponent (n) and the plane strain (PS) forming limit (FLC_0) for $\sigma^* = K$. Here the forming limits in uniaxial tension (UT) and balanced biaxial tension (BB) are constant (UT: ε_1 = 1.0, ε_2 = -0.5; BB: ε_1 = 0.5, ε_2 = 0.5). At n = 1 (linear FLC), FLC_0 is 0.75, and as $n \rightarrow \infty$, FLC_0 approaches the value 0.8660 = $(3/4)^{0.5}$. The relationships in Figure 3 apply only to the chosen material model and the proposed failure criterion.

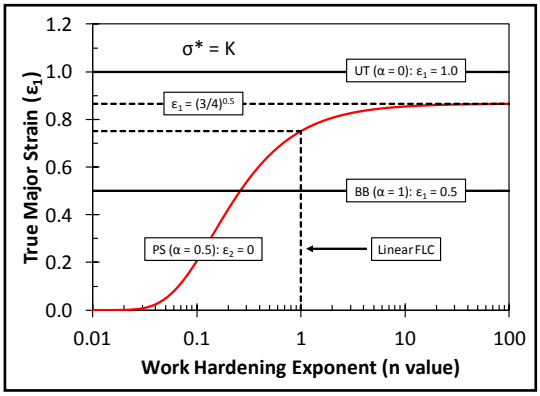

Figure 3. Theoretical effect of the work hardening exponent (n) on the plane strain (PS) forming limit (FLC_0) for σ^* = K. The constant major strain values for uniaxial tension (UT) and balanced biaxial tension (BB) stress states are shown for reference. See text for details.

2.3. Extension beyond the tension-tension quadrant

The critical normal stress failure criterion is identical in form to several other established failure criteria within the tension-tension plane-stress quadrant (Figure 2). The difference is that the proposed criterion is applied to localized necking rather than to yielding or fracture. The Mohr-Coulomb (M-C) criterion [25]-[26] was developed in the context of soil and rock mechanics and is commonly used to describe the fracture response of brittle materials to combined shear and normal stresses. Over the past decade, Bai and Wierzbicki [27] have pioneered the application of the M-C criterion to ductile fracture—*i.e.* the Modified Mohr-Coulomb (MMC) fracture model. The classic M-C criterion indicates that failure will occur at a critical combination of shear stress (τ) and normal stress (σ_n), or

$$\tau + c_1\sigma_n = c_2, \tag{6}$$

where c_1 and c_2 are material constants. For c_1 = 0, the M-C criterion reduces to the Tresca maximum shear stress criterion [28]. At the other extreme is the Rankine criterion [29], where it is assumed that failure will occur when the maximum principal stress at any point reaches a critical value.

Figure 4 is a schematic Mohr's circle representation that illustrates the possible effects of compression on the proposed localized necking failure criterion. In Figure 4a, uniaxial tension (UT) is shown for reference, where the failure criterion is met at $\sigma_1 = \sigma^*$ and $\tau_{max} = \sigma^*/2$. In this case the Mohr-Coulomb, Tresca and Rankine criteria are equivalent. The anticipated effects of superposed uniaxial compression (UC) are shown in Figure 4b (Tresca), Figure 4c (Rankine) and Figure 4d (M-C). The UC component may be imagined either as an in-plane compressive stress (*e.g.* deep drawing or shear) or as a tooling contact stress normal to the sheet surface. For the Tresca criterion, the maximum shear stress at failure is the same as in uniaxial tension ($\tau_{max} = \sigma_1/2$), but the maximum normal stress is less than the critical normal stress ($\sigma_1 < \sigma^*$). For the Rankine criterion, the maximum normal stress at failure is the same as in uniaxial tension ($\sigma_1 = \sigma^*$), and the maximum shear stress is larger ($\tau_{max} > \sigma^*/2$). For the Mohr-Coulomb criterion, the maximum shear stress at failure is larger than in uniaxial tension ($\tau_{max} > \sigma^*/2$), while the maximum normal stress is smaller ($\sigma_1 < \sigma^*$).

At this time the authors make no explicit assumptions regarding the most appropriate form of the proposed failure criterion outside the tension-tension quadrant. In the context of incremental sheet forming, Emmens *et al.* [30] explained that the strain-based FLC is only valid with certain restrictions, namely: (A) linear strain path, (B) absence of bending, (C) absence of through-thickness shear, and (D) plane-stress condition. They commented further that both shear and contact stresses change the

stress state and that both lower the yield stress in tension and raise the necking limit. Recently Min *et al.* [31] presented a methodology to compensate for the combined effects of curvature, non-linear strain path and contact pressure when contrasting strain-based FLCs measured with Nakajima-type tooling and Marciniak-type tooling. They showed that with proper consideration, the Nakajima-type FLC (curvature, non-linear strain path, contact pressure) reduced to the Marciniak-type FLC (in-plane deformation, quasi-linear strain path, no contact pressure).

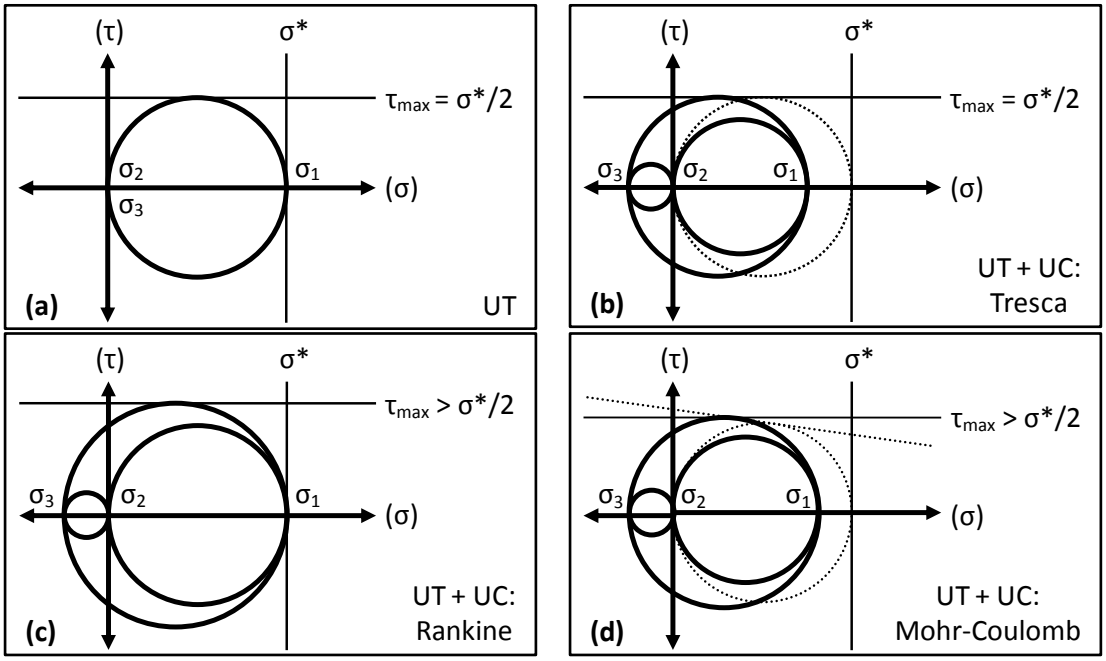

Figure 4. Mohr's circle representation illustrating the effects of compression on the proposed failure criterion: UT = uniaxial tension; UC = uniaxial compression. See text for details.

3. Materials and procedures

3.1. Materials

Four 980 Class AHSS materials were considered in this analysis, and the basic tensile properties are listed in Table 2. All materials were produced through cold-rolling at U. S. Steel Gary Works in Gary, IN, USA and finished at the PRO-TEC Coating Company continuous annealing line in Leipsic, OH, USA. Materials A and B are conventional multi-phase steels, where "HY" indicates a high yield strength version (*i.e.* 980-HY), and for Material B "(LCE)" indicates a low carbon equivalent. Material C (980 TBF) is a TRIP-assisted bainite/ferrite steel (TRIP = transformation-induced plasticity). Material D (USS 980 GEN3) is a third generation advanced high strength steel or "3rd GEN AHSS" [32] with an exceptional combination of strength and ductility. Here the prefix "USS" indicates a specific type of 3rd GEN AHSS manufactured exclusively by United States Steel Corporation.

Table 2. Basic tensile properties[a]

ID	Material	t, mm	YS, MPa	UTS, MPa	UE, %	TE, %
A	980-HY	1.4	714	1040	8.5	14.0
B	980-HY (LCE)	1.5	764	1042	6.4	11.4
C	980 TBF	1.4	863	1081	8.5	12.9
D	USS 980 GEN3	1.4	655	1020	16.7	21.6

[a] ASTM standard [33]; transverse orientation; t = nominal thickness; YS = yield strength; UTS = ultimate tensile strength; UE = uniform elongation; TE = total elongation

3.2. Strain-based forming limit measurements

Experimental strain-based forming limits were measured according to ISO Standard 12004-2 [34]. A Marciniak-type punch and carrier blank configuration was used with a digital image correlation (DIC) strain measurement system. In contrast to a Nakazima-type hemispherical (dome) punch, the Marciniak configuration eliminates specimen curvature and friction in the area of interest and provides a nearly linear (proportional) strain path to failure [35]. For each material six specimen types (widths) were utilized to achieve a range of strain paths, and three specimens were tested for each specimen type. Further details regarding the experimental method are given by Huang and Shi [36].

3.3. Determining the critical normal stress (σ^*)

It is well-known that diffuse necking begins at maximum load during a uniaxial tension test [37]. At this critical moment, the work hardening rate $(d\sigma/d\varepsilon)$ is equal to the true flow stress (σ), and, for power law work hardening, the work hardening exponent (n) is equal to the true strain (ε), or

$$\left(\frac{d\sigma}{d\varepsilon} = \sigma\right) \rightarrow \left(nK\varepsilon^{n-1} = K\varepsilon^{n}\right) \rightarrow (n = \varepsilon). \tag{7}$$

The subscript "u" may be used to designate "ultimate load" (or UTS or uniform elongation). As such, n_{u} is the work hardening exponent at maximum load, and σ_{u} is the true stress at maximum load, and K_{u} is the strength coefficient at maximum load, where

$$n_{\mathrm{u}} = \varepsilon_{\mathrm{u}} = \ln\left(1 + \frac{UE,\%}{100}\right);\ \ \sigma_{\mathrm{u}} = UTS\left(1 + \frac{UE,\%}{100}\right);\ \ K_{\mathrm{u}} = \frac{\sigma_{\mathrm{u}}}{(n_{\mathrm{u}})^{n_{\mathrm{u}}}}. \tag{8}$$

Upon rearranging Equation 5 and substituting $n_{\mathrm{u}}, K_{\mathrm{u}}$ for n, K, the critical normal stress (σ^*) is:

$$\sigma^* = \frac{K_{\mathrm{u}}}{A}\exp\left[\frac{\ln(\varepsilon_1 B)}{n_{\mathrm{u}}}\right]. \tag{9}$$

3.4. Constructing the Model FLC

The nearest-to-plane-strain (NTPS) forming limit (ε_2 closest to zero) is used to "anchor" or calibrate the model to the experimental strain-based FLC. Equation 9 is solved for the NTPS forming limit to find the critical normal stress. Subsequently the Model FLC is constructed by applying Equation 5 for various stress states ranging from α = 0 (UT) through α = 1 (BB) with n and K equal to n_{u} and K_{u}, respectively. The basic procedure to construct the Model FLC is summarized in Table 3.

Table 3. Procedure to construct the Model FLC

Step	Description: Comments
1	Tension test: Determine σ_{u}, n_{u} and K_{u}
2	Measure experimental FLC: Determine the NTPS forming limit[a]
3	Calculate σ^*: Solve Equation 9 for the NTPS forming limit
4	Construct Model FLC: Apply Equation 5 ($\alpha = 0 \rightarrow 1; n, K = n_{\mathrm{u}}, K_{\mathrm{u}}$)
[a] NTPS = nearest to plane strain (ε_2 closest to zero)	

As a practical matter, the NTPS data are typically at or near the minimum of the strain-based FLC, and the corresponding major strain values are not exorbitantly different from the uniform elongation (UE) in magnitude (Equation 8). As such, extrapolation from the UE value in tension to the plane strain forming limit should be more accurate than if the calibration were performed in another deformation mode with much larger major strain values—*e.g.* uniaxial tension or balanced biaxial stretching. The authors credit an anonymous manuscript reviewer for this rather astute observation.

4. Results and discussion

4.1. Strain-based FLCs

Strain-based forming limit diagrams are presented in Figure 5, where experimental forming limits and the Model FLC are shown for each material. The Model FLC adequately describes the experimental forming limit data in three of four cases (materials A, B, C). For material D (USS 980 GEN3), the Model FLC generally under-predicts the forming limit for biaxial stretching conditions ($\varepsilon_2 > 0$).

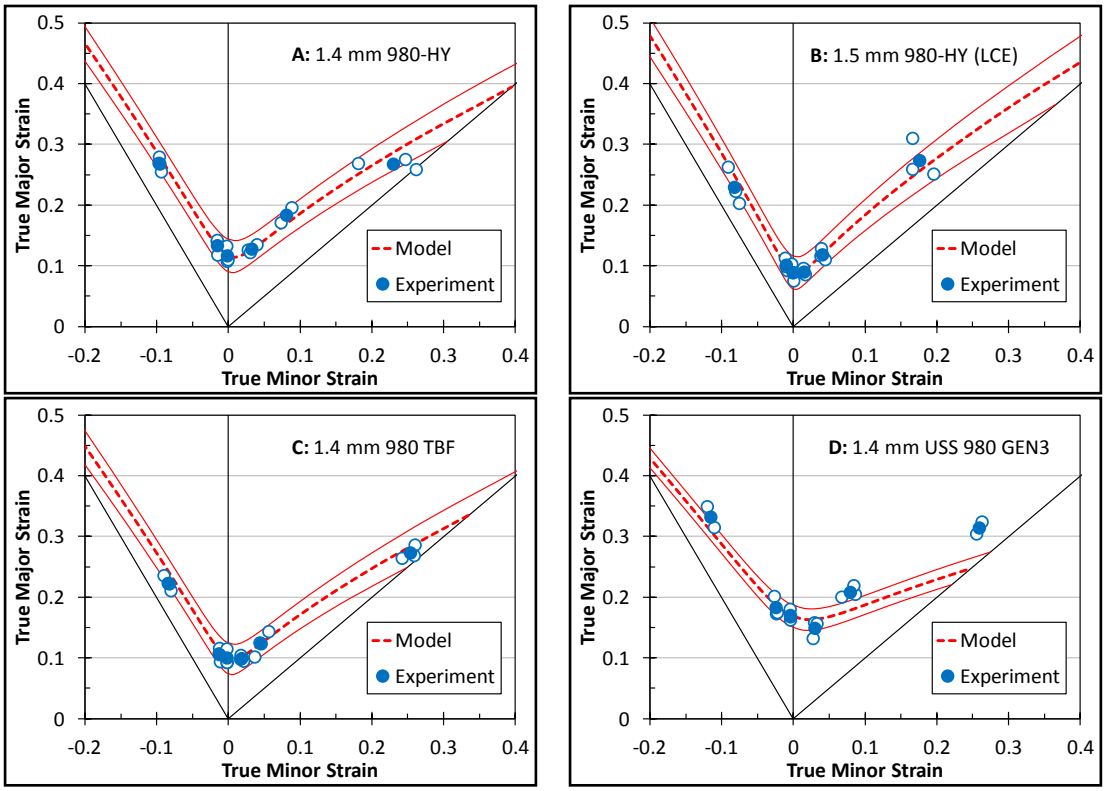

Figure 5. Forming limit diagrams for materials A through D. For each case, the heavy, dashed curve is the FLC derived from the critical normal stress criterion (Model FLC). The Model FLC is anchored by the nearest-to-plane-strain (NTPS) experimental forming limit. The thin, continuous curves define 95% confidence bands based on the NTPS forming limit data (±2σ, n=3). Filled symbols (●): Average for each specimen type; Unfilled symbols (○): Individual test results.

The microstructure of USS 980 GEN3—like most other third generation advanced high strength steels—contains a substantial amount of austenite (> 10%). As such this material derives exceptional properties in part from the TRIP effect (transformation-induced plasticity), where metastable austenite transforms into martensite during deformation. As the proposed methodology appears suitable for conventional AHSS materials, it is likely that special consideration will be required for materials with higher levels of retained austenite. While material C (980 TBF) is considered a "TRIP-assisted" AHSS, the amount of retained austenite is much lower (< 5%) than that of USS 980 GEN3.

4.2. Property relationships

The ultimate load properties (Equation 8) and the critical normal stress (Equation 9) for each material are listed in Table 4. It was observed that the ratio σ^*/σ_u is around 1.2 for all four materials. Also, for materials A, B and C, the ratio σ^*/K_u is greater than 0.95, while that of material D is 0.90. As a reminder, for power law work hardening (Equation 4), the strength coefficient (K) is equivalent to the effective stress ($\bar{\sigma}$) at an effective strain ($\bar{\varepsilon}$) of 1.0. As such, the ratio σ^*/K_u is an important indicator of

relative behavior. If this ratio is lower, the critical normal stress is reached "sooner", with respect to K_u. If this ratio is higher, localized necking is deferred to a higher relative stress value.

Table 4. Model FLC parameters: Critical normal stress criterion

ID	Material	t mm	n_u	σ_u MPa	K_u MPa	σ^* MPa	σ^*/σ_u	σ^*/K_u
A	980-HY	1.4	0.081	1128	1383	1357	1.20	0.98
B	980-HY (LCE)	1.5	0.062	1109	1316	1321	1.19	1.00
C	980 TBF	1.4	0.082	1173	1439	1393	1.19	0.96
D	USS 980 GEN3	1.4	0.154	1190	1587	1424	1.20	0.90

Figure 5 shows a strong linear relationship between the critical normal stress (σ^*) and the measured true stress at maximum load (σ_u) over a range of strength levels. The 780 and 1180 Class AHSS materials were evaluated in a separate analysis [36]. This empirical functionality suggests the basis for a simple methodology by which strain-based FLCs may be estimated from a standard tension test.

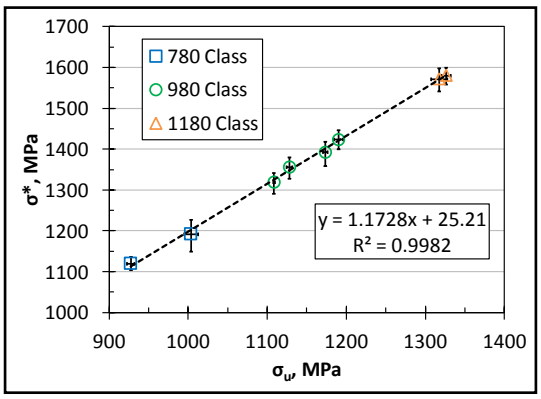

Figure 6. Linear relationship between the critical normal stress (σ^*) and the measured true stress at maximum load in a tension test (σ_u) over a range of strength levels. Average values for the 980 Class AHSS materials are listed in Table 4.

4.3. Outlook

Considering the simplifying assumptions made, the results of this analysis are very encouraging. A more sophisticated material model, an adapted failure criterion, and/or an alternative strain-based FLC measurement method would affect the observed relationships. Other uncertainties in the current analysis include the proportionality of the imposed strain paths, variation in tensile properties and the suitability of the strain-based forming limit measurement system itself. Further development of this concept may include: extension beyond the plane-stress tension-tension quadrant; extension to Nakajima-type testing; consideration of critical normal stress anisotropy in relation to measured tensile properties and forming limits (*e.g.* rolling direction vs. transverse direction); and further consideration of the effects of retained austenite in third generation advanced high strength steels.

5. Summary and conclusions

A methodology for stress-based forming limit analysis has been developed for advanced high strength steel (AHSS). It was proposed that localized necking occurs when a critical normal stress condition is met. Using a basic, isotropic material model (von Mises yield function, power law hardening), the criterion was applied to four 980 Class AHSS materials. The following conclusions were drawn:

1. The proposed stress-based failure criterion adequately described the experimental strain-based forming limit data in three of four cases.
2. For third generation AHSS materials with substantial volume fractions of metastable austenite, a more sophisticated material model and/or an adapted failure criterion will be required.

3. A strong linear relationship was found between the critical normal stress (σ^*) and the measured true stress at maximum load in tension (σ_u). This empirical functionality applies over a large range of strength levels and may form the basis for a methodology by which FLCs can be estimated from standard tension tests.

Acknowledgment and disclaimer
The authors would like to thank United States Steel Corporation for permission to publish this manuscript. Thanks also go to Dr. Thomas B. Stoughton of General Motors for helpful discussions.

References

[1] Stoughton T B and Yoon J W 2014 Stress-based forming limit curves *Assessing Properties of Conventional and Specialized Materials* (*Comprehensive Materials Processing* vol 1) ed C J Van Tyne (Amsterdam: Elsevier) chapter 4 pp 71-84
[2] Keeler S P and Backhofen W A 1964 Plastic instability and fracture in sheet stretched over rigid punches *ASM Trans. Q*, **56** pp 25-48
[3] Nakazima N, Kikuma T and Hasuka K 1968, Study on the formability of steel sheets, *Yamata Technical Report* **264** pp 8517-30
[4] Kleemola H J and Pelkkikangas M T 1977 Efect of predeformation and strain path on the forming limits of steel, copper and brass *Sheet Met. Ind.* **64** pp 591-9
[5] Arrieux R, Bedrin C and Boivin M 1982 Determination of an intrinsic forming limit stress diagram for isotropic metal sheets *Proc. 12th Biennial Congress of the International Deep Drawing Research Group (IDDRG)* pp 61-71
[6] Nhat T N and Arrieux R 1995 Off-axes forming-limit stress diagrams of an anisotropic steel sheet *J. Mat. Proc. Tech.* **54** pp 193-8.
[7] Stoughton T B 2000 A general forming limit criterion for sheet metal forming *Int. J. Mech. Sci.* **42** pp 1-27
[8] Matin P H, Smith L M and Petrusevski S 2006 A method for stress space forming limit digram construction for aluminum alloys *J. Mater. Proc. Tech.* 174 pp 258-65
[9] Wu P D, Graf A, MacEwan S R, Lloyd D J, Jain M and Neale K W 2005 On forming limit stress diagram analysis *Int. J. Solids Struct.* **42** pp 2225-41
[10] Kinsey B and Sakash A 2006 Evaluation of stress saturation effect with a stress based failure criterion for sheet metal using numerical simulations *SAE Tech. Paper Ser.* 2006-01-0350
[11] Zhou L, Xue K-M and Li P 2007 Determination and application of stress-based forming limit diagram in aluminum tube hydroforming *Trans. Nonferrous Met. Soc. China* **17** pp 21-6
[12] Stoughton T B and Yoon J W 2011 A new approach for failure criterion for sheet metals *Int. J. Plasticity* **27** pp 440-59
[13] Stoughton T B and Yoon J W 2012 Path independent forming limits in strain and stress space *Int. J. Solids Struct.* **49** pp 3616-25
[14] Carr A R, Walker A and Combaz E 2013 Derivation of a forming limit stress diagram from an experimental FLC, and comparison of the two criteria when applied to FE simulation of a pressing using different yield functions *Int. J. Mater. Form.* **8** pp 45-57
[15] Kolasangiani K, Shariati M and Farhangdoost K 2015 Prediction of forming limit curves (FLD, MSFLD and FLSD) and necking time for SS304L sheet usibng finite element method and ductile fracture criteria J. Comput. Appl. Res. Mech. Eng. **4** pp 121-32
[16] Panich S, Liewald M and Uthaisangsuk V 2017 Stress and strain based fracture forming limit

curves for advanced high strength steel sheet *Int. J. Mater Form* pp 1-19
[17] Stoughton T B 2002 The influence of the material model on the stress-based forming limit criterion *SAE Tech. Paper Ser.* 2002-01-0157
[18] Sing W M and Rao K P 1993 Prediction of sheet metal formability using tensile test results *J. Mater. Process Technol.* 37 pp 37-51
[19] Stören S and Rice J R 1975 Localized necking in thin sheets *J. Mech. Phys. Solids* **23** pp 421-41
[20] Needleman A and Rice J R 1978 Limits to ductility set by plastic flow localization *Mechanics of Sheet Metal Forming* ed D P Koistinen and N-M Wang (New York: Plenum Press) pp 237-68
[21] Paul S K 2013 Theoretical analysis of strain- and stress-based forming limit diagrams *J. Strain Analysis* **48** pp 177-88
[22] Sadagopan S and Urban D 2003 *AISI/DOE Technology Roadmap Program: Formability Characterization of a New Generation of High Strength Steels* (Pittsburgh: AISI)
[23] Sriram S, Huang G, Yan B and Geoffroy J-L 2009 Comparison of forming limit curves for advanced high strength steels using different techniques *SAE Int. J. Mater. Manuf.* **2** pp 472-81
[24] Frómeta D, Tedesco M, Calvo J, Lara A, Molas S and Casellas S 2017 Assessing edge cracking resistance in AHSS automotive parts by the essential work of fracture methodology *J. Phys. Conf. Ser.* **896** 012102
[25] Coulomb C A 1776 Essai sur une application des règles des maximis et minimis à quelques problèmes de statique, relatifs à l'architecture *Mém. Math. et Phys. – Académie Roy. des Sciences* **7** pp 343-87
[26] Mohr O 1900 Welche Umstande bedingen die Elastizitatsgrenze und den Bruch eines Materials *Zeitschrift des Vereins Deutscher Ingenieure Band* **44** pp 1524-30
[27] Bai Y L and Wierzbicki T 2010 Application of the extended Mohr-Coulomb criterion to ductile fracture *Int. J. Fracture* **161** pp 1-20
[28] Tresca H 1864 Mémoires sur l'écoulement des corps solides soumis a de fortes pressions *C. R. Acad. Sci. Paris* 59 pp 754-8
[29] Rankine W 1857 On the stability of loose earth *Phil. Trans. Royal Soc. London* **147** pp 9-27
[30] Emmens W C, van der Weijde D H and van den Boogaard A H 2009 The FLC, enhanced formability, and incremental sheet forming *Proc. International Deep Drawing Research Group International Conference (IDDRG)* pp 773-84
[31] Min J, Stoughton T B, Carsley J E and Lin J 2016 Compensation for process-dependent effects in the determination of localized necking limits *Int. J. Mech. Sci.* **117** pp 115-34
[32] WorldAutoSteel 2017 *Advanced High-Strength Steels Application Guidelines Version* 6.0 ed Keeler S, Menachem K and Mooney P (www.worldautosteel.org)
[33] ASTM International 2015 *Standard Test Methods for Tension Testing of Metallic Materials* E8/E8M – 15a
[34] International Organization for Standardization 2008 *Metallic Materials – Sheet and Strip – Determination of Forming-Limit Curves – Part 2: Determination of Forming-Limit Curves in the Laboratory* 12004-02
[35] Leppin C, Li J and Daniel D 2008 Application of a method to correct the effect of non-proportional strain paths on Nakajima test based forming limit curves *Proc. 7th International Conference and Workshop on Numerical Simulation of 3D Sheet Metal Forming Processes (NUMISHEET)* pp 217-22
[36] Huang L and Shi M F 2018 Forming limit curves of advanced high strength steels: Experimental determination and empirical prediction," *SAE Tech. Paper Ser.* 2018-01-0804
[37] Hosford W F and Caddell R M 1983 *Metal Forming: Mechanics and Metallurgy* (Englewood Cliffs, New Jersey: Prentice-Hall)